Engineering Notes

ENGINEERING NOTES are short manuscripts describing new developments or important results of a preliminary nature. These Notes cannot exceed 6 manuscript pages and 3 figures; a page of text may be substituted for a figure and vice versa. After informal review by the editors, they may be published within a few months of the date of receipt. Style requirements are the same as for regular contributions (see inside back cover).

Optimal Trajectories for a Ballistic Re-entry Vehicle Recovery System

Walton E. Williamson Jr.*
Sandia Laboratories, Albuquerque, N.Mex.

Nomenclature

C_D = drag coefficient
$C_{D_{max}}$ = maximum value of drag coefficient
$C_{D_{min}}$ = minimum value of drag coefficient
G = function to be minimized
h, V = state variables (altitude, velocity)
H = variational Hamiltonian
q' = dynamic pressure $= 0.5\rho V^2$
S = reference area divided by mass
t, τ = independent variables (t = time)
u = control variable
β, ρ_E = constants for exponential density model
γ = flight path angle
λ_h, λ_v = Lagrange multipliers for optimal control problem

Subscripts
0 = evaluated at the initial value of the independent variable
f = evaluated at the final value of the independent variable

Introduction

In a previous paper,[1] a scheme for determining design parameters for a recoverable re-entry vehicle was described. This involved selecting timer settings to determine the mass jettison and parachute deployment times for a re-entry vehicle which would insure recovery of the vehicle in spite of the uncertainty in its drag coefficient history. The scheme involved determining upper and lower limits for the drag coefficient history and then computing drag coefficient histories inside the boundaries which would result in worst-case trajectories. The design parameters (timer settings) were then selected to keep the worst-case trajectories inside acceptable design limits. The "worst-case" trajectories for the recovery problem occurred when the dynamic pressure at parachute deployment was either a minimum or a maximum. Since parachute deployment was determined by a timer, trajectories which produce minimum or maximum dynamic pressure for a fixed final time were needed. Note that, if the dynamic pressure at chute deployment is either too high or too low, the chute may not open properly. The results in Ref. 1 showed that the drag coefficient history, which resulted in worst-case trajectories, contained a jump from one boundary (upper or lower) to the other boundary (lower or upper) at some intermediate time. These results are not consistent with the simple solutions presented in Ref. 2 where "worst-case" trajectories would not seem to have jumps in the drag coefficient history.

The purpose of this paper is to demonstrate analytically why the drag coefficient history which results in minimum or maximum dynamic pressure at parachute deployment can contain jumps and also to show that the results shown in Ref. 1 are consistent with those shown in Ref. 2. This was accomplished by first formulating and solving the optimization problem which extremizes dynamic pressure at a fixed final time. These results are consistent with using a timer to determine the parachute deployment event. The problem is then reformulated using altitude as the independent variable and the fixed final altitude problem is solved. These results are consistent with Ref. 2. The results show that, if the final time is fixed, jumps can occur in the optimal drag coefficient history. If the final altitude is fixed, jumps do not occur.

Analysis

The problem may be stated as follows: Given a set of initial conditions for a re-entry vehicle and bounds for the drag coefficient history, determine the drag coefficient history which produces maximum (or minimum) dynamic pressure at specified end conditions. If a simple dynamic model is used for re-entry, then the jump conditions are easy to see. Thus, the state equations for re-entry are chosen to be

$$\dot{h} = V\sin\gamma \qquad \dot{V} = -q'SC_D \tag{1}$$

These equations assume that the re-entry vehicle may be modeled as a point mass, that rotational and gravitational effects of the Earth are not important, and that the flight path angle is constant during re-entry. An exponential atmospheric density profile is assumed so that $\rho = \rho_E e^{-\beta h}$ and the speed of sound is assumed to be constant.

The problem of maximizing the dynamic pressure at a specified final time is solved first. In order to formulate all problems as minimization problems, the performance index is written as

$$G = -q'_f \tag{2}$$

and the end condition requires t_f to be fixed. The optimal control problem is specified by the preceding information and the bounds for C_D. The bounds for C_D are assumed to be a function of Mach number and typical bounds used in the example in this paper are shown in Ref. 3. This is a standard optimal control problem and solution techniques are described in Ref. 4. Here the control variable is first transformed to an unconstrained control by

$$C_D = \left(\frac{C_{D_{max}} - C_{D_{min}}}{2}\right)\sin u + \left(\frac{C_{D_{max}} + C_{D_{min}}}{2}\right) \tag{3}$$

where $C_{D_{max}}$ and $C_{D_{min}}$ are functions of Mach number and u is an unconstrained control variable. Defining the Hamiltonian as

$$H = \lambda_h(V\sin\gamma) + \lambda_v(-q'SC_D) \tag{4}$$

Presented as Paper 78-1366 at the AIAA Atmospheric Flight Mechanics Conference, Palo Alto, Calif., Aug. 7-9, 1978; submitted Aug. 31, 1978; revision received April 27, 1979.

Index category: Entry Vehicle Dynamics and Control.

*Member of Technical Staff, Aeroballistics Projects Division. Member AIAA.

the additional first-order necessary conditions which a minimizing solution must satisfy are

$$\dot{\lambda}_h = -\frac{\partial H}{\partial h} = -\beta\lambda_v q' S C_D \tag{5a}$$

$$\dot{\lambda}_v = -\frac{\partial H}{\partial V} = -\lambda_h \sin\gamma + \lambda_v \rho S\left(VC_D + \tfrac{1}{2}V^2\frac{\partial C_D}{\partial V}\right) \tag{5b}$$

and

$$H_u = -\lambda_v q' S\left[\frac{C_{D_{\max}} - C_{D_{\min}}}{2}\right]\cos u = 0 \tag{6}$$

The boundary conditions on the Lagrange multipliers are

$$\lambda_{h_f} = +\beta q'_f \qquad \lambda_{v_f} = -\rho_f V_f \tag{7}$$

This completes the definition of the necessary conditions which a solution to the optimal control problem must satisfy. The solution to this two-point boundary value problem provides the C_D history which produces maximum dynamic pressure.

The optimal control is determined from Eq. (6). Singular arc solutions, $\lambda_v = 0$, are not possible. This is shown in Ref. 3. Thus, Eq. (6) requires $u = \pm\pi/2$. This implies that the optimal control must remain on a boundary and the optimal solution will consist of boundary segments satisfying the two-point boundary value problem described earlier.

For a minimal solution

$$H_{uu} = \lambda_v q' S\left[\frac{C_{D_{\max}} - C_{D_{\min}}}{2}\right]\sin u \geq 0 \tag{8}$$

Thus, if $\lambda_v < 0$, then $u = -\pi/2$ and, if $\lambda_v > 0$, then $u = \pi/2$.

Equation (7) requires $\lambda_{v_f} < 0$ at the final time so that C_D at the final point is on the lower boundary. If λ_v can change signs, however, then C_D can jump to the upper boundary. It is easy to show that sign changes in λ_v can occur, if the time interval between t_0 and t_f is sufficiently large. This is discussed in Ref. 3. Thus, boundary jumps are certainly possible when the independent variable is time and extremal solutions are computed over a fixed time interval.

An example problem is solved to show the effect of the change in sign of λ_v. The constants for the example problem and the bounds for C_D are shown in Ref. 3. The multiplier histories are shown in Fig. 1 and indicate that C_D is on the upper boundary for 2.8 s. It then switches to the lower boundary. The dynamic pressure history is shown in Fig. 2. Figure 2 also shows dynamic pressure histories which occur when either the lower boundary or the upper boundary for C_D is used. The final value of the dynamic pressure is 11013, 10508, and 6259 lb/ft^2 for each of the three trajectories, respectively. It can be seen that the optimal solution has a smaller peak dynamic pressure than the trajectory using $C_{D_{\min}}$. This causes the optimal solution to have a higher velocity later in the trajectory and the dynamic pressure histories finally cross. Thus, the boundary jump does increase the value of the dynamic pressure at the specified final time.

If the minimum dynamic pressure problem is formulated, Eqs. (2) and (7) change signs. This just reverses the signs on the multipliers. Hence, the solution is on the upper boundary at the final time, but may switch to the lower boundary, if λ_v changes signs.

The problem will now be reformulated using altitude as the independent variable. In order to avoid an independent variable, which is not monotonically increasing, τ is defined such that

$$\frac{d\tau}{dt} = V \qquad \frac{dV}{d\tau} = -\tfrac{1}{2}S\rho V C_D \tag{9}$$

The variable τ is used instead of h since τ is monotonically increasing. It is related to altitute by $(\tau - \tau_0)\sin\gamma = h - h_0$. Thus, a given value of h_f specifies τ_f.

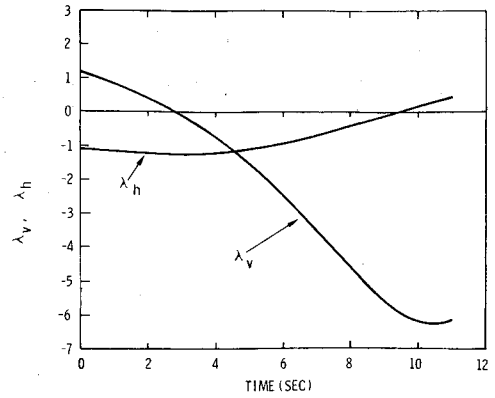

Fig. 1 Lagrange multiplier histories for example problem.

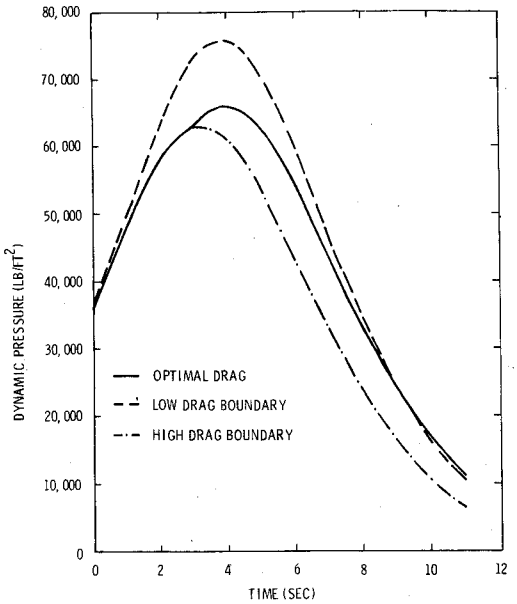

Fig. 2 Dynamic pressure histories for example problem.

Only one state variable [Eq. (9b)] is required here. The following equations help define the optimal solution

$$\frac{d\lambda_v}{d\tau} = \left[\tfrac{1}{2}S\rho\left(C_D + V\frac{\partial C_D}{\partial V}\right)\right]\lambda_v \tag{10a}$$

$$\lambda_{v_f} = -\rho_f V_f \tag{10b}$$

and

$$\frac{\partial H}{\partial u} = \left(-\tfrac{1}{2}S\rho V\right)\lambda_v\left(\frac{C_{D_{\max}} - C_{D_{\min}}}{2}\right)\cos u = 0 \tag{11a}$$

$$\frac{\partial^2 H}{\partial u^2} = \left(\tfrac{1}{2}S\rho V\right)\lambda_v\left(\frac{C_{D_{\max}} - C_{D_{\min}}}{2}\right)\sin u \geq 0 \tag{11b}$$

Equation (11a) requires that either $u = \pm\pi/2$ or $\lambda_v = 0$. Singular arc solutions with $\lambda = 0$ will not occur since the generalized convexity condition shown in Ref. 5 can never be satisfied. Thus, $u = \pm\pi/2$ where the sign on u is determined from Eq. (11b). If $\lambda_v < 0$, then $u = -\pi/2$ and, if $\lambda_v > 0$, then $u = \pi/2$. At the final time, λ_{v_f} is negative. The solution to Eq. (10a) is

$$\lambda_v = \lambda_{v_f}\exp\left\{\int_{\tau_f}^{\tau}\left[\tfrac{1}{2}S\rho\left(C_D + V\frac{\partial C_D}{\partial V}\right)\right]d\xi\right\} \tag{12}$$

and hence, the sign of λ_v can never change. Thus, the solution is always on the lower boundary, as would be predicted by the solutions shown in Ref. 2.

This can also be shown by freeing the final time and fixing the final altitude in the first formulation. The solution obtained in this manner is discussed in Ref. 3 and is shown to provide the same results as those just given.

Summary

The optimal control problem, to determine the drag coefficient history inside of upper and lower bounds, which produces maximum or minimum values of dynamic pressure at specified final end conditions for a ballistic re-entry vehicle has been formulated. The results indicate that, if the final time is fixed, then the optimal solutions may contain jumps in the control variable from one boundary to the other. If the final altitude is fixed, then the optimal solutions will not contain jumps. These results are consistent with results published earlier which indicate that jumps in the drag coefficient should not occur, if the altitude is used as the independent variable. If the final state of a re-entry vehicle trajectory segment is to be determined by a timer, however, then a design scheme which attempts to determine trajectories with minimum or maximum dynamic pressure must consider possible jumps in the drag coefficient history.

Acknowledgments

This work was supported by the Department of Energy.

References

[1] Williamson, W. E., "An Automated Scheme to Determine Design Parameters for a Recoverable Re-entry Vehicle," *Journal of Spacecraft and Rockets,* Vol. 14, Aug. 1977, pp. 496-500.

[2] Allen, H. J. and Eggers, A. E., "A Study of the Motion and Aerodynamic Heating of Ballistic Missiles Entering the Earth's Atmosphere at High Supersonic Speeds," NACA Rep. 1381, 1958.

[3] Williamson, W. E., "Optimal Drag Coefficient Histories Which Extremize Dynamic Pressure for a Ballistic Reentry Vehicle," AIAA Paper 78-1366, Atmospheric Flight Mechanics Conference, Palo Alto, Calif., Aug. 7-9, 1978.

[4] Bryson, A. E. and Ho, Y. C., *Applied Optimal Control,* Blaisdell Publishing Co., Waltham, Mass., 1969.

[5] Kelley, H. J., Kopp, R. E., and Moyer, A. G., "Singular, Extremals," *Topics in Optimization,* edited by G. Leitmann, Vol. II, Academic Press, New York, 1966, Chapt. 3.

In-Flight Simulation with Pilot-Center of Gravity Offset and Velocity Mismatch

Robert F. Stengel*
Princeton University, Princeton, N.J.

Nomenclature

$\boldsymbol{a}$ = body-axis acceleration vector
a_y = lateral acceleration component
$\boldsymbol{C_B}$ = feedback gain matrix
$\boldsymbol{C_F}$ = forward gain matrix
$\boldsymbol{F}$ = fundamental (stability) matrix
$\boldsymbol{G}$ = control effect matrix
$\boldsymbol{g}$ = gravitational acceleration vector
g = gravitational acceleration magnitude
$\boldsymbol{H}_E^B$ = Earth-to-body-axis transformation matrix
$L_{(\ )}$ = roll stability and control derivatives
$N_{(\ )}$ = yaw stability and control derivatives
p = roll rate
r = yaw rate
$\boldsymbol{T}$ = similarity transformation matrix
t = time
$\boldsymbol{U}$ = control transformation matrix
V = velocity magnitude
$\boldsymbol{v}$ = body-axis velocity vector
$\mathbf{x}$ = body-axis position vector
x = axial position
$\boldsymbol{x}$ = state vector
$Y_{(\ )}$ = side-force stability and control derivatives
z = vertical position
β = sideslip angle
$\boldsymbol{\delta}$ = control vector
δA = aileron angle
δR = rudder angle
δSF = side-force panel angle
ϕ = roll angle
$\boldsymbol{\omega}$ = body-axis angular rate vector
$\tilde{\omega}$ = cross-product equivalent matrix

Received Jan. 29, 1979; revision received June 15, 1979.

Index categories: Handling Qualities, Stability and Control; Simulation; Flight Operations.

*Associate Professor, Dept. of Mechanical and Aerospace Engineering. Associate Fellow AIAA.

Introduction

TWO objectives for in-flight simulation of one aircraft by another are matching the modal characteristics of the model and duplicating its response to command inputs. Six-degree-of-freedom in-flight simulators, such as the Princeton Variable-Response Research Aircraft (VRA) and the USAF/Calspan Total In-Flight Simulator (TIFS), can provide "perfect" model following (in the sense of Erzberger[1]) for rigid-body modes and responses. However, if there is airspeed mismatch or difference in the pilot's location relative to the rotational center, then perfect following of the model's state variables is no guarantee of an acceptable simulation. The pilot's acceleration cues, which are central to flying qualities evaluation, are certain to be different from those of the model. In such instance, it becomes necessary to modify the simulation control logic so that accelerations at the pilot's station are matched at the expense of mismatch in cues which are secondary to the simulated piloting task. If the model is realized explicitly in the simulator's control system, airspeed and pilot location mismatch effects can be compensated by transforming the outputs of the system's model equations before they are transmitted to the model-following logic.[2-4] If implicit model following (or "response feedback") is used, it is necessary to transform the model itself prior to generating the implicit model-following control gains.

A solution for airspeed and pilot station mismatch is found by performing a sequential similarity transformation on the linear differential equations which describe model dynamics. For lateral acceleration matching, the simplest procedure is to accommodate pilot station effects by transforming model sideslip angle, while velocity mismatch is compensated through yaw rate transformation. Normal acceleration matching can be accomplished through similar transformations of model angle of attack and pitch rate, and it is not discussed further. In either case, the similarity transformation preserves model eigenvalues while matching acceleration cues. The model transformation for lateral acceleration matching is developed, and an example based on VRA simulation of the Space Shuttle is presented.

Implicit Model Following

Given the linear-time-invariant dynamic model of the aircraft to be simulated,

$$\Delta\dot{x}_M = F_M \Delta x_M + G_M \Delta\delta_M \qquad \Delta x_M(0) = \Delta x_0 \qquad (1)$$

the objective is to find feedback and forward gain matrices, C_B and C_F, which cause the simulation aircraft's modes and responses to mimic the model. The simulation aircraft's rigid-body motions are represented by

$$\Delta\dot{x}_S = F_S\Delta x_S + G_S\Delta\delta_S \qquad \Delta x_S(0) = \Delta x_0 \qquad (2)$$

The perturbation state vectors (Δx_M and Δx_S) are n-dimensional, the model control ($\Delta\delta_M$) has l components, and the simulator control ($\Delta\delta_S$) has m components. For the complete aircraft equations, $n > m \geq l$.

With identical initial conditions, the model and simulator motions are the same when $\Delta\dot{x}_M = \Delta\dot{x}_S$; this establishes the criterion for "perfect" model following. In the equivalent stability derivative (ESD) approach, the state rates are identically matched[1]; using linear-quadratic implicit model following, the state rates are matched in a least-squares sense.[5] The two methods produce identical control structures and gain matrices when the "perfect" model-following criterion is satisfied and when there are not added constraints on control usage or parameter insensitivity.

The stability-axis state vectors of the lateral-directional model and the simulator each take the form,

$$\Delta x^T = (\Delta r\ \Delta\beta\ \Delta p\ \Delta\phi)$$

and their fundamental matrices contain the aircraft's dimensional stability derivatives. Neglecting unsteady aerodynamic effects,

$$F = \begin{bmatrix} N_r & N_\beta & N_p & 0 \\ (Y_r/V - 1) & Y_\beta/V & Y_p/V & g/V \\ L_r & L_\beta & L_p & 0 \\ 0 & 0 & 1 & 0 \end{bmatrix} \qquad (3)$$

Note that the fourth rows of F_M and F_S are necessarily identical. Consequently, a three-component control vector, $\Delta\delta_S^T = (\Delta\delta R\ \Delta\delta SF\ \Delta\delta A)_S$, can provide "perfect" model following, subject to control actuator limitations. The corresponding control effect matrix is

$$G_S = \begin{bmatrix} N_{\delta R} & N_{\delta SF} & N_{\delta A} \\ Y_{\delta R}/V & Y_{\delta SF}/V & Y_{\delta A}/V \\ L_{\delta R} & L_{\delta SF} & L_{\delta A} \\ 0 & 0 & 0 \end{bmatrix}_S \qquad (4)$$

The model's control vector may not contain $\Delta\delta SF$, in which case $\Delta\delta_M$ has two components, and G_M is redefined accordingly.

Because the fourth rows of the model and simulator equations are identical, they can be neglected in determining the "perfect" model-following control law. The model and simulator state rates are equal when

$$F'_M\Delta x_M + G'_M\Delta\delta_M = F'_S\Delta x_S + G'_S\Delta\delta_S \qquad (5)$$

where the prime denotes a truncated (three-row) matrix. When the model and simulator are matched, $\Delta x_M = \Delta x_S$, and the ESD control law is derived from Eq. (5):

$$\Delta\delta_S = G_S'^{-1}[(F'_M - F'_S)\Delta x_S + G'_M\Delta\delta_M]$$

$$= C_B\Delta x_S + C_F\Delta\delta_M \qquad (6)$$

This "perfect" model-following control law is seen to include state feedback (through C_B) and command-input interconnect (through C_F). The elements of the closed-loop simulator matrices are equivalent to the stability derivatives of the model:

$$\Delta\dot{x}_S = (F_S + G_S C_B)\Delta x_S + G_S C_F\Delta\delta_M = F_M\Delta x_S + G_M\Delta\delta_M \qquad (7)$$

Lateral Acceleration Matching

The body-axis acceleration vector at the pilot's station is

$$a_P = \dot{v}_P - H_E^B g + (\tilde{\omega}\tilde{\omega} + \dot{\tilde{\omega}})(x_P - x_{cg}) \qquad (8)$$

Recognizing that stability axes are a special set of body axes (nominally oriented to the velocity vector), neglecting coupling between longitudinal and lateral-directional motions, and assuming that the pilot's station is on the aircraft's plane of symmetry, perturbations in lateral acceleration are described by

$$\Delta a_{y_P} = V(\Delta\dot{\beta} + \Delta r) + g\Delta\phi + (x_P - x_{cg})\Delta\dot{r} - (z_P - z_{cg})\Delta\dot{p} \qquad (9)$$

With differing velocity or pilot offset, one or more simulator state variables must be altered to provide the Δa_{y_P} match. This is most readily accomplished by transforming a different state variable for each type of acceleration mismatch.

Consider first the model transformation for pilot-center of gravity (c.g.) offset at identical airspeeds. Three states (Δr, Δp, and $\Delta\phi$) are to be matched identically. Defining $x = x_P - x_{cg}$, model and simulator lateral acclerations are matched when

$$V_M\Delta\dot{\beta}_S + x_S\Delta\dot{r}_M - z_S\Delta\dot{p}_M = V_M\Delta\dot{\beta}_M + x_M\Delta\dot{r}_M - z_M\Delta\dot{p}_M \qquad (10)$$

Rearranging Eq. (10) and integrating once provides $\Delta\beta_S$, and the model state vector which the simulator should follow to compensate for differing pilot-c.g. offsets is

$$\begin{bmatrix} \Delta r \\ \Delta\beta \\ \Delta p \\ \Delta\phi \end{bmatrix}_{M_l} = \begin{bmatrix} 1 & 0 & 0 & 0 \\ \dfrac{(x_M - x_S)}{V_M} & 1 & \dfrac{-(z_M - z_S)}{V_M} & 0 \\ 0 & 0 & 1 & 0 \\ 0 & 0 & 0 & 1 \end{bmatrix} \begin{bmatrix} \Delta r \\ \Delta\beta \\ \Delta p \\ \Delta\phi \end{bmatrix}_M \qquad (11)$$

or $\Delta x_{M_l} = T_l\Delta x_M$. T_l is a similarity transformation matrix; therefore, the model eigenvalues can be preserved in writing Eq. (1) with Δx_{M_l} as the state vector:

$$\Delta\dot{x}_{M_l} = T_l F_M T_l^{-1}\Delta x_{M_l} + T_l G_M\Delta\delta_M = F_{M_l}\Delta x_{M_l} + G_{M_l}\Delta\delta_M \qquad (12)$$

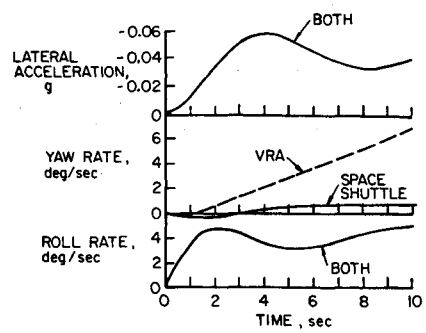

Fig. 1 Comparison of SSV and VRA response, with lateral acceleration matching.

Table 1 Implicit model-following gains for VRA simulation of SSV

	C_B				C_F	
	Δr_S	$\Delta\beta_S$	Δp_S	$\Delta\phi_S$	$\Delta\delta R_M$	$\Delta\delta A_M$
			without lateral acceleration matching			
$\Delta\delta R_S$	0.071	−1.057	0.057	0.033	0.095	0.051
$\Delta\delta SF_S$	−0.018	−0.556	−0.014	0.383	−0.002	−0.017
$\Delta\delta A_S$	0.034	−0.139	−0.295	−0.021	0.059	0.226
			with lateral acceleration matching			
$\Delta\delta R_S$	0.165	−0.483	0.081	−0.014	0.095	0.051
$\Delta\delta SF_S$	−0.041	0.928	−0.020	0.003	−0.002	−0.017
$\Delta\delta A_S$	0.019	−0.238	−0.299	0.004	0.059	0.226

Next, consider the model transformation for velocity mismatch with no pilot-c.g. offset. With $\Delta\beta$, Δp, and $\Delta\phi$ matched identically,

$$V_S(\Delta\dot{\beta}_M + \Delta r_S) = V_M(\Delta\dot{\beta}_M + \Delta r_M) \tag{13}$$

or

$$\Delta r_S = (V_M/V_S - 1)\Delta\dot{\beta}_M + (V_M/V_S)\Delta r_M \tag{14}$$

Substituting for $\Delta\dot{\beta}_M$ using Eqs. (1), (3), and (5),

$$\Delta r_s = \left(1 + \frac{Y_{r_M}}{V_S} - \frac{Y_{r_M}}{V_M}\right)\Delta r_M + \left(\frac{V_M}{V_S} - 1\right)\left(\frac{Y_{\beta_M}}{V_M}\Delta\beta_M + \frac{Y_{p_M}}{V_M}\Delta p + \frac{g}{V_M}\Delta\phi_M + \frac{Y_{\delta R_M}}{V_M}\Delta\delta R_M + \frac{Y_{\delta SF_M}}{V_M}\Delta\delta SF_M + \frac{Y_{\delta A_M}}{V_M}\Delta\delta A_M\right) \tag{15}$$

The model state transformation for velocity mismatch incorporates Eq. (15) for the modeled yaw rate in T_2 and U_2, and $\Delta x_{M_2} = T_2\Delta x_M + U_2\Delta\delta_M$. The transformed model's dynamic equation is

$$\Delta\dot{x}_{M_2} = T_2F_MT_2^{-1}\Delta x_{M_2} + T_2(G_M - F_MT_2^{-1}U_2)\Delta\delta_M + U_2\Delta\dot{\delta}_M \tag{16}$$

Since U_2 contains only side-force control terms, it often would be negligible. In this case, applying the velocity mismatch transformation to the offset-corrected model [Eq. (12)] leads to

$$\Delta\dot{x}_{M_2} = T_2T_1F_MT_1^{-1}T_2^{-1}\Delta x_{M_2} + T_2T_1G_M\Delta\delta_M = F_{M_2}\Delta x_{M_2} + G_{M_2}\Delta\delta_M \tag{17}$$

with $\Delta x_{M_2} = T_2T_1\Delta x_M$. This is the model which should be followed by the in-flight simulator for lateral acceleration matching.

Velocity Mismatch Example

An example based upon VRA simulation of the Space Shuttle vehicle (SSV) is presented, considering only the velocity mismatch between the two vehicles.[6] The SSV flight condition is $M = 1.5$ at an altitude of 18,300 m (60,000 ft); the VRA is assumed to perform the in-flight simulation at an airspeed of 105 knots and an altitude of 1500 m (5,000 ft). Open-loop response of the SSV to a 1°-differential elevon step input results in a maximum lateral acceleration of 0.05 g at $t = 4$ s. Without lateral acceleration matching, the in-flight simulator can match the state response with negligible error; however, as a result of the velocity mismatch, Δa_y is 0.24 g at $t = 4$ s and growing steadily. The VRA can match lateral acceleration precisely (as well as $\Delta\beta$, Δp, and $\Delta\phi$) by following a transformed yaw rate (Fig. 1). Response in the first few seconds after the pilot's command is of greatest importance, and roll control is the primary SSV piloting task at this flight condition; therefore, the difference in VRA and SSV yaw responses should not have a major effect on flying qualities assessment.

The effect of Δa_y matching on ESD gains is of interest; Table 1 presents C_B and C_F for the two cases. Feedback gains are changed substantially, but Δa_y has no significant effect on control interconnects. The most notable effects are on sideslip and roll angle feedback to rudder and side-force panel, as might be expected.

Conclusion

Similarity transformations which preserve modal characteristics and acceleration cues in in-flight simulation are presented. A velocity-mismatch example illustrates that acceleration matching is achieved at the expense of mismatching in cues which are secondary to the simulated piloting task, while primary cues are preserved. The approach is applicable for both implicit and explicit model following, and it can be easily extended to the longitudinal case.

Acknowledgments

This work was sponsored in part by NASA Langley Research Center under Contract No. NAS1-13502.

References

[1] Erzberger, H., "Analysis and Design of Model Following Control Systems by State Space Techniques," *Proceedings of the 1968 Joint Automatic Control Conference,* June 1968, pp. 572-581.

[2] Reynolds, P.A., Wasserman, R., Fabian, G.J., and Motyka, P.R., "Capability of the Total In-Flight Simulator," Air Force Flight Dynamics Lab, Wright-Patterson Air Force Base, Ohio, AFFDL-TR-72-39, July 1972.

[3] Reynolds, P.A., Schelhorn, A.E., and Wasserman, R., "Drive Logic for In-Flight Simulators," AIAA Paper 73-933, Sept. 1973.

[4] Keller, R.L., Lowell, N., and Williams, J.F., "Digital Avionics System for the Shuttle Training Aircraft," AIAA Paper 77-1529, Nov. 1977.

[5] Tyler, J.S., Jr., "The Characteristics of Model-Following Systems as Synthesized by Optimal Control," *IEEE Transactions on Automatic Control,* Vol. AC-9, Oct. 1964, pp. 485-498.

[6] Stengel, R.F. and Miller, G.E., "Flying Qualities of an Aircraft with Strong Lateral-Directional Coupling," AIAA Paper 78-1361, Aug. 1978.